

ACCEPTED MANUSCRIPT • OPEN ACCESS

Variation in atomistic structure due to annealing at diamond/silicon heterointerfaces fabricated by surface activated bonding

To cite this article before publication: Yutaka Ohno *et al* 2022 *Jpn. J. Appl. Phys.* in press <https://doi.org/10.35848/1347-4065/ac5d11>

Manuscript version: Accepted Manuscript

Accepted Manuscript is “the version of the article accepted for publication including all changes made as a result of the peer review process, and which may also include the addition to the article by IOP Publishing of a header, an article ID, a cover sheet and/or an ‘Accepted Manuscript’ watermark, but excluding any other editing, typesetting or other changes made by IOP Publishing and/or its licensors”

This Accepted Manuscript is © 2022 The Author(s). Published by IOP Publishing Ltd..

As the Version of Record of this article is going to be / has been published on a gold open access basis under a CC BY 3.0 licence, this Accepted Manuscript is available for reuse under a CC BY 3.0 licence immediately.

Everyone is permitted to use all or part of the original content in this article, provided that they adhere to all the terms of the licence <https://creativecommons.org/licenses/by/3.0>

Although reasonable endeavours have been taken to obtain all necessary permissions from third parties to include their copyrighted content within this article, their full citation and copyright line may not be present in this Accepted Manuscript version. Before using any content from this article, please refer to the Version of Record on IOPscience once published for full citation and copyright details, as permissions may be required. All third party content is fully copyright protected and is not published on a gold open access basis under a CC BY licence, unless that is specifically stated in the figure caption in the Version of Record.

View the [article online](#) for updates and enhancements.

Variation in atomistic structure due to annealing at diamond/silicon heterointerfaces fabricated by surface activated bonding

Yutaka Ohno^{1*}, Jianbo Liang², Hideto Yoshida³, Yasuo Shimizu^{4, 5}, Yasuyoshi Nagai⁴, Naoteru Shigekawa²

¹*Institute for Materials Research (IMR), Tohoku University, 2-1-1 Katahira, Aoba-ku, Sendai 980-8577, Japan*

²*Graduate School of Engineering, Osaka-City University, 3-3-138 Sugimoto, Sumiyoshi, Osaka 558-8585, Japan*

³*SANKEN, Osaka University, 8-1 Mihogaoka, Ibaraki, Osaka 567-0047, Japan*

⁴*Institute for Materials Research (IMR), Tohoku University, 2145-2 Narita-cho, Oarai, Ibaraki 311-1313, Japan*

⁵*National Institute for Materials Science, 1-2-1 Sengen, Tsukuba 305-0047, Japan*

E-mail: yutaka.ohno.e6@tohoku.ac.jp

Abstract

Chemical composition around diamond/silicon heterointerfaces fabricated by surface activated bonding at room temperature is examined by energy dispersive X-ray spectroscopy under scanning transmission electron microscopy. Iron impurities segregate just on the bonding interfaces, while oxygen impurities segregate off the bonding interfaces in the silicon side by 3-4 nm. Oxygen atoms would segregate so as to avoid the amorphous compound with silicon and carbon atoms, self-organized at the bonding interfaces in the surface activated bonding process. When the bonding interfaces are annealed at 1000 °C, the amorphous compound converts into cubic silicon carbide (c-SiC), and nano-voids 5-15 nm in size are formed at the region between silicon and c-SiC, at which the oxygen density is high before annealing. The nano-voids can act as the gettering sites in which metal impurities are preferentially agglomerated, and the impurity gettering would help to improve the electronic properties of the bonding interfaces by annealing.

1. Introduction

Diamond crystals have superior physical properties towards high power, high frequency, and low-loss electronic devices,¹⁾ for which the figures of merit are extremely high.²⁾ They have wide bandgap, high carrier mobility,³⁾ high saturation velocity,⁴⁾ and the highest electrical breakdown field strength,⁵⁾ that are suitable for power electronics.^{6, 7)} Also, they have high thermal conductivity,⁸⁾ that are suitable for superior heat spreaders of power devices for the next generation applications beyond 5G,⁹⁾ as demonstrated in heterointerfaces between diamond and gallium nitride (GaN)^{10, 11)} or silicon (Si)^{12, 13)}. Although high-quality monocrystalline diamond wafers are commercially available,^{14, 15)} their surface size is rather small ($< 15 \times 15 \text{ mm}^2$) and they are still expensive for device manufacturing. A possible solution is bonding diamond chips with an inexpensive Si wafer, that would be effective for developing electronics application.^{16, 17)}

In order to design high-performance power devices, the thermal stability of diamond/Si bonding interfaces is an important issue, because the interfaces are exposed to high temperatures during device fabrication and operation processes. Diamond/Si bonding interfaces with a high crystallinity, free from adhesive intermediate layers, can be fabricated by fusion bonding at elevated temperatures above $1150 \text{ }^\circ\text{C}$ ¹⁸⁾ and by hydrophilic bonding at about $200 \text{ }^\circ\text{C}$ ^{19, 20)}. However, the interfaces would be cracked at elevated temperatures due to a large thermal expansion coefficient mismatch, and therefore mechanical and thermal properties of the interfaces would be degraded via the structural modification. Similar interfaces can be fabricated using adhesive metallic layers,²¹⁾ that could suppress the structural modification at elevated temperatures. However, the metallic layers can act as an impurity source, and electronic properties of the interfaces could be degraded via the migration of metallic impurities at elevated temperatures.

Recently, it is shown that diamond/Si heterointerfaces fabricated by surface activated bonding (SAB) at room temperature (RT) are not cracked even after $1000 \text{ }^\circ\text{C}$ annealing,¹⁷⁾ via some kind of stress relaxation.²²⁾ This mechanical stability against thermal processes is attributed to a composition-graded amorphous layer with carbon and silicon atoms self-organized in the bonding process.²³⁾ According to the model, the amorphous compound is crystallized forming cubic silicon carbide (c-SiC) during $1000 \text{ }^\circ\text{C}$ annealing, and the crystallized layer would suppress the concentration of thermal stresses at the interface and consequently keep the crack-free interface in thermal processes.²³⁾ Meanwhile, impacts of compositional modification around the interfaces by annealing, including impurity diffusion, on electronic properties are not fully examined, even though the diamond devices fabricated

on the interfaces are operated well.¹⁶⁾ In the present work, we have examined the chemical composition around the interfaces, and discussed how the impacts of impurity atoms can be suppressed.

2. Experimental methods

A diamond/Si heterointerface was fabricated by SAB with a square wafer (4 mm x 4 mm x 0.65 mm in size) of high-pressure, high-temperature synthetic Ib type (100) monocrystalline diamond and a rectangular wafer (12 mm x 10 mm x 0.52 mm) of (100) n-Si ($2.6 \times 10^{16} \text{ mm}^{-3}$).¹⁷⁾ The wafers were activated at RT in a high vacuum (below $5 \times 10^{-5} \text{ Pa}$) using an argon (Ar) atom beam with a current of 1.65 mA at an applied voltage of 1.6 kV. The activated wafers were then pressed each other for bonding immediately after the activation process. The exact location of the bonding interface was determined with iron (Fe) impurities introduced intentionally in the surface activation process.²⁴⁾ A part of the bonding interface was annealed at 1000 °C for 12 h in a nitrogen gas ambient.¹⁶⁾

Specimens with the interface for scanning transmission electron microscopy (STEM) were fabricated using the following steps. A thick foil (more than a few micrometers thick) with the diamond/Si heterointerface was cut out by using a conventional focused ion beam (FIB) system, equipped with a high-resolution scanning electron microscope (SEM) (FEI, Helios NanoLab600i),²⁵⁾ and mounted on a lift-out grid for STEM. The surface normal for Si side was $\langle 110 \rangle$, while that for diamond side was $\langle 100 \rangle$. Then, the foil was thinned by FIB milling operated at low temperatures (LT-FIB), since the conventional FIB milling operated at RT (RT-FIB) easily introduce structural defects at SAB-fabricated interfaces.^{26,}²⁷⁾ The foil was thinned to about 100 nm thick by LT-FIB milling with a cold stage operated at -150°C (IZUMI-TECH, IZU-TSCS004) to suppress the structural modification in the FIB processes.^{24, 27-29)}

The chemical composition around the interface was examined by energy dispersive X-ray spectroscopy (EDX) under STEM, using a JEOL JEM-ARM200F analytical microscope. The impurity detection limit was about 0.1 at.%. The atomic arrangement around the interface was examined by high-angle annular dark-field (HAADF-) STEM using a JEM-ARM200F microscope with the atomic resolution of about 0.12 nm.

3. Results and discussion

3.1 As-bonded interfaces

STEM-EDS reveals atomic intermixing across the interface in the bonding process at RT

(Figs. 1(a) and 1(b)).³⁰⁾ A composition-graded amorphous layer with carbon and Si atoms is formed via the intermixing (Fig. 1(f)), that is attributed to a transient enhanced diffusion due to the mobile vacancies introduced in the surface activation process.²³⁾ Except for the host elements of carbon and Si, there exist Fe,³¹⁾ Ar, and oxygen atoms around the bonding interface (Figs. 1(c)-(d)), and no other impurity atom is detected. It is known that Fe atoms are introduced just on the activated surfaces during the surface activation process, and they slightly diffuse during the bonding process, presumably via the transient enhanced effect.²⁴⁾ The half-width at half-maximum (HWHM) of the Fe distribution, estimated to be 1 nm, is independent of the specimen thickness, even though the spatial resolution of STEM-EDX would depend on the specimen thickness via the spread of electron beam. This suggests that the spatial resolution of our STEM-EDX is less than 1 nm, and the estimated resolution is consistent with the previous report²⁴⁾. As indicated with the green curve in Fig. 1(f), Fe atoms can diffuse by 2-3 nm in the Si side from the bonding interface. This diffusion length is almost the same as the diffusion length estimated in the SAB-fabricated Si/GaAs²⁴⁾ and Si/Si²⁷⁾ interfaces, suggesting the same diffusion mechanism in the bonding process. Similarly, the density of Ar atoms, that are inevitably introduced during the surface activation process, is maximum at the bonding interface, and the Ar density profile across the interface is almost the same morphology as the Fe density profile (the pink curve in Fig. 1(f)). These results would support the transient enhancement diffusion model that the diffusion lengths of those impurities are dominated by the diffusivity of the point defects assisting the impurity diffusion.²⁹⁾

On the other hand, the oxygen density peaks off the bonding interface in the Si side by 3-4 nm (the yellow curve in Fig. 1(f)). Since oxygen atoms can be observed in any SAB-fabricated interfaces, they would be introduced from the residual gas molecules containing oxygen, such as water and oxygen molecules, in the vacuum chamber. At similar SAB-fabricated interfaces such as GaAs/Si,³²⁾ diamond/GaN,³³⁾ diamond/aluminum,³⁴⁾ and diamond/copper,²⁵⁾ the oxygen density peaks just on the bonding interfaces. Meanwhile, the oxygen density at the SAB-fabricated diamond/Si interface seems to have a negative correlation with the excess number of carbon atoms in the Si side (the blue curve in Fig. 1(f)), that are related to an amorphous layer with carbon and Si atoms self-organized in the surface activated bonding process.²³⁾ Since the solubility of oxygen in silicon carbide is rather low,³⁵⁾ oxygen atoms would be kicked out from the bonding interface via the self-organization of the amorphous compound with carbon and Si atoms.

3.2 1000 °C annealed interfaces

1
2
3 When the bonding interface is annealed at 1000 °C, spherical defects about 5-15 nm in
4 size are formed in the Si side (Fig. 2(a)). The defects locate inside the Si matrix just on the
5 interface between Si and c-SiC (Fig. 2(b)), introduced via the crystallization of the
6 amorphous compound with carbon and Si atoms by annealing [23]. At dark spherical defects
7 in HAADF-STEM images, the number density of Si atoms is decreased while carbon atoms
8 are scarcely observed (see Figs. 2(b) to 2(d)). This indicates that the defects would be the
9 nanometer-sized agglomerates of lattice vacancies, i.e., nano-voids in Si.

10
11 At bright spherical defects in HAADF-STEM images, Fe atoms are observed and the
12 number density of Si atoms is slightly decreased (see Figs. 2(b), 2(c), and 2(e)). No Fe
13 agglomerate is observed at the region free from nano-voids, within the detection limit of our
14 STEM-EDS (Fig. 2(e)). These results suggest that Fe atoms would agglomerate inside nano-
15 voids and/or Fe agglomerates are nucleated nearby nano-voids. Therefore, nano-voids would
16 act as gettering sites for Fe atoms. It is shown that electronic properties of SAB-fabricated
17 Si/diamond heterojunction diodes, such as ideality factor, reverse-bias current, and barrier
18 height at Si/diamond bonding interfaces, are improved by post-bonding annealing,
19 presumably via the reduction of interface states that are formed during the SAB processes.³⁶⁾
20 Isolated metal atoms including Fe and point defects, introduced during the surface activation
21 process, can induce defect levels around the bonding interfaces. Meanwhile, metal
22 agglomerates with a moderate size do not affect the electronic properties so much.³⁷⁾
23 Gettering of metallic impurities including Fe into nano-voids, as well as the recovery of
24 crystallinity around the bonding interface,²³⁾ would help to reduce the interface states.

25
26 Oxygen atoms also impact on the electronic properties when they form precipitates (such
27 as oxides) and defect clusters (such as oxygen-vacancy agglomerates) by annealing, while
28 they are electronically inactive when they are isolated. The impacts would be small at the
29 annealed diamond/Si interfaces, since oxygen atoms do not segregate around the interfaces
30 including nano-voids (Fig. 2(f)).

31
32 Figure 2(g) shows that Ar atoms can segregate at nano-voids, as well as at the c-SiC layer,
33 in which the crystallinity is still decreased.²³⁾ Similar Ar segregation into a damaged layer at
34 a SAB-fabricated interface is reported.³⁸⁾ It is hypothesized that inert Ar atoms would
35 segregate so as to fill the vacant spaces at nano-voids and at the vacant defects introduced
36 during the surface activation process. Agglomerates of inert Ar atoms would not impact on
37 the electronic properties, while they may impact on the thermal properties of the interfaces.

38
39 Finally, we briefly discuss the formation process of nano-voids. Similar nano-voids
40 acting as the gettering sites for Fe and Ar atoms are formed at the Si/Si homointerfaces

1
2
3 fabricated by SAB with the same bonding condition (Fig. 3). Unlike at the diamond/Si
4 heterointerfaces, the nano-voids are formed just on the bonding interface, at which the
5 oxygen density is maximum. The results in Figs. 2 and 3 suggest that nano-voids are formed
6 at the region in which a number of oxygen atoms exist. It is hypothesized that oxygen would
7 assist the void formation, by producing joint vacancy-oxygen agglomerates (oxide particles)
8 and by trapping vacancies into VO₂ clusters, as proposed in Czochralski-grown Si ingots.³⁹⁾
9 Moreover, nano-voids at the diamond/Si interfaces (5-15 nm in size) are much larger in
10 comparison with the Si/Si interfaces (less than 5 nm in size). It is known that voids are self-
11 organized at the Si/SiC interfaces during the carbonization of Si crystals,⁴⁰⁾ and the volume
12 of the voids per unit area is proportional to the oxygen density.⁴¹⁾ Although the formation
13 mechanism is still controversial, the void formation would be correlated with the growth of
14 c-SiC and oxygen impurities.
15
16
17
18
19
20
21
22
23
24
25

26 **4. Conclusions**

27 Chemical composition around SAB-fabricated diamond/Si heterointerfaces is examined by
28 STEM-EDS combined with LT-FIB. Fe and Ar impurities segregate just on the bonding
29 interfaces, while oxygen impurities segregate off the bonding interfaces in the Si side by 3-
30 4 nm, so as to avoid the amorphous compound with carbon and Si atoms introduced at the
31 bonding interfaces. After 1000 °C annealing, nano-voids are formed at the region where the
32 oxygen density is high before bonding. They would act as the gettering sites for metal
33 impurities, and the impurity gettering would help to improve the electronic properties of the
34 interfaces by annealing.
35
36
37
38
39
40
41
42

43 **Acknowledgments**

44 This work was supported by JSPS/KAKENHI, Grant No. 21H01830 (SAB), JST/CREST,
45 Grant No. JPMJCR17J1 (LT-FIB), the GIMRT Program in IMR, Tohoku University, Grant
46 Nos. 202012-IRKMA-0412 and 202012-IRKMA-0046 (LT-FIB), and the NJRC Program in
47 SANKEN, Osaka University, Grant No. 20211245 (STEM-EDS).
48
49
50
51
52

53 **References**

- 54
55
56 1) C.J.H. Wort, *Mat. Today* **11**, 22 (2008).
57 2) H. Umezawa, M. Nagase, Y. Kato, and S. Shikata, *Diam. Relat. Mater.* **24**, 201 (2012).
58 3) J. Isberg, J. Hammersberg, E. Johansson, T. Wikström, D.J. Twitchen, A.J. Whitehead, S.E.
59 Core, and G.A. Scarsbrook, *Science* **297**, 1670 (2002).
60

- 4) F. Nava, C. Canali, C. Jacoboni, L. Reggiani, and S.F. Kozlov, *Solid State Commun.* **33**, 475 (1980).
- 5) H. Umezawa, T. Matsumoto, and S. Shikata, *IEEE Electron Device Lett.* **35**, 1112 (2014).
- 6) T. Matsumoto, H. Kato, K. Oyama, T. Makino, M. Ogura, D. Takeuchi, T. Inokuma, N. Tokuda, and S. Yamasaki, *Sci. Rep.* **6**, 31585 (2016).
- 7) T. Iwasaki, Y. Hoshino, K. Tsuzuki, H. Kato, T. Makino, M. Ogura, D. Takeuchi, T. Matsumoto, H. Okushi, S. Yamasaki, and M. Hatano, *Appl. Phys. Express* **5**, 091301 (2012).
- 8) D.J. Twitchen, C.S.J. Pickles, and C.E. Hall, *Diam. Relat. Mater.* **10**, 731 (2001).
- 9) Z. Ren, J. Xu, X. Le, and C. Lee, *Micromachines* **12**, 946 (2021).
- 10) Y. Zhou, R. Ramaneti, and M. Kuball, *Appl. Phys. Lett.* **111**, 141901 (2017).
- 11) A.J. Trindade, B. Guilhabert, and M.D. Dawson, *Opt. Express* **23**, 9329 (2015).
- 12) Y. Han, B.L. Lau, and K.F. Choo, *IEEE Trans. Compon. Packaging Manuf. Technol.* **4**, 983 (2014).
- 13) A. Aleksov, X. Li, and Z. Sitar, *Diam. Relat. Mater.* **14**, 308 (2005).
- 14) H. Aida, S.W. Kim, K. Ikejiri, Y. Kawamata, K. Koyama, H. Kodama, and A. Sawabe, *Appl. Phys. Express* **9**, 035504 (2016).
- 15) H. Yamada, A. Chayahara, Y. Mokuno, H. Umezawa, and S. Shikata, *Appl. Phys. Express* **3**, 051301 (2010).
- 16) J. Liang, S. Masuya, S. Kim, T. Oishi, M. Kasu, and N. Shigekawa, *Appl. Phys. Express* **12**, 016501 (2019).
- 17) J. Liang, S. Masuya, M. Kasu, and N. Shigekawa, *Appl. Phys. Lett.* **110**, 111603 (2017).
- 18) G.N. Yushin, S.D. Wolter, A.V. Kvit, R. Collazo, B.R. Stoner, J.T. Prater, and Z. Sitar, *Appl. Phys. Lett.* **81**, 3275 (2002).
- 19) T. Matsumae, Y. Kurashima, H. Takagi, and H. Umezawa, *Scr. Mater.* **191**, 52 (2021).
- 20) T. Matsumae, Y. Kurashima, H. Umezawa, and H. Takagi, *Scr. Mater.* **175**, 24 (2020).
- 21) T. Matsumae, Y. Kurashima, H. Umezawa, Y. Mokuno, and H. Takagi, *Microelectron. Eng.* **195**, 68 (2018).
- 22) J. Liang, Y. Zhou, S. Masuya, F. Guemann, M. Singh, J. Pomeroy, S. Kim, M. Kuball, M. Kasu, and N. Shigekawa, *Diam. Relat. Mater.* **93**, 187 (2019).
- 23) Y. Ohno, J. Liang, H. Yoshida, Y. Shimizu, Y. Nagai, and N. Shigekawa, submitted.
- 24) Y. Ohno, J. Liang, N. Shigekawa, H. Yoshida, S. Takeda, R. Miyagawa, Y. Shimizu, and Y. Nagai, *Appl. Surf. Sci.* **525**, 146610 (2020).
- 25) S. Kanda, Y. Shimizu, Y. Ohno, K. Shirasaki, Y. Nagai, M. Kasu, N. Shigekawa, and J. Liang, *Jpn. J. Appl. Phys.* **59**, SB3B03 (2020).

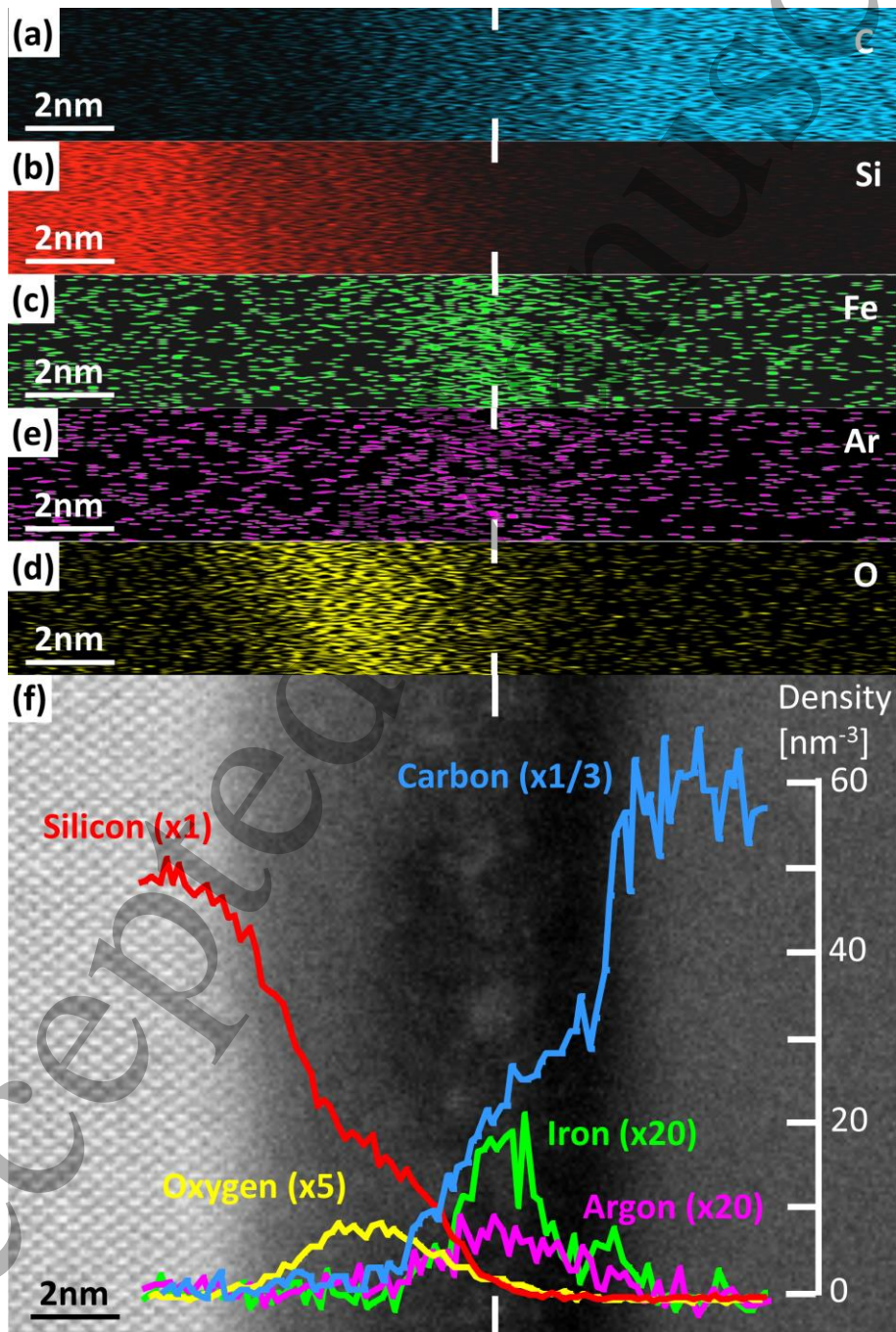
- 26) Y. Ohno, H. Yoshida, S. Takeda, J. Liang, and N. Shigekawa, *Jpn. J. Appl. Phys.* **57**, 02BA01 (2018).
- 27) Y. Ohno, H. Yoshida, N. Kamiuchi, R. Aso, S. Takeda, Y. Shimizu, Y. Nagai, J. Liang, and N. Shigekawa, *Jpn. J. Appl. Phys.* **59**, SBBB05 (2020).
- 28) Y. Ohno, J. Ren, S. Tanaka, M. Kohyama, K. Inoue, Y. Shimizu, Y. Nagai, and H. Yoshida, *Appl. Phys. Express* **14**, 041003 (2021).
- 29) Y. Ohno, T. Yokoi, Y. Shimizu, J. Ren, K. Inoue, Y. Nagai, K. Kutsukake, K. Fujiwara, A. Nakamura, K. Matsunaga, and H. Yoshida, *Sci. Technol. Adv. Mater. Methods* **1**, 169 (2021).
- 30) Y. Ohno, J. Liang, H. Yoshida, Y. Shimizu, Y. Nagai, and N. Shigekawa, *Proc. 7th Int. IEEE Workshop Low Temperature Bonding for 3D Integration* **2021**, 12.
- 31) It should be noted that, by using a proper surface activation condition [ref. 24], the concentration of metallic impurities from the susceptors can be reduced to be lower than the detection limit of atom probe tomography (about 0.01 at.%).
- 32) R. Huang, T. Lan, C. Li, J. Li, and Z. Wang, *Chin. Phys. B* **30**, 076802 (2021).
- 33) J. Liang, A. Kobayashi, Y. Shimizu, Y. Ohno, S.W. Kim, K. Koyama, M. Kasu, Y. Nagai, and N. Shigekawa, *Adv. Mater.* **33**, 2104564 (2021).
- 34) J. Liang, S. Yamajo, M. Kuball, and N. Shigekawa, *Scripta Mater.* **159**, 58 (2019).
- 35) M. Di Ventura and S.T. Pantelides, *J. Electron. Mater.* **29**, 353 (2000).
- 36) Y. Uehigashi, S. Ohmagari, H. Umezawa, H. Yamada, J. Liang, and N. Shigekawa, *Diam. Relat. Mater.* in press.
- 37) T. Buonassisi, A.A. Istratov, M.A. Marcus, B. Lai, Z. Cai, S.M. Heald, and E.R. Weber, *Nature Mater.* **4**, 676 (2005).
- 38) S. Yang, Y. Qu, N. Deng, K. Wang, S. He, Y. Yuan, W. Hu, S. Wu, and H. Wang, *Mater. Res. Express* **8**, 085901 (2021).
- 39) V.V. Voronkov, *J. Crystal Growth* **310**, 1307 (2008).
- 40) C.J. Mogab and H.J. Leamy, *J. Appl. Phys.* **45**, 1075 (1974).
- 41) A. Leycuras, *Appl. Phys. Lett.* **70**, 1533 (1997).

Figure Captions

Fig. 1. Spatial distribution of (a) carbon, (b) Si, (c) Fe, (d) Ar, and (e) oxygen atoms around the bonding interface. The height of each map is reduced to 1/4. (f) Density profiles across the interface for carbon (the blue curve), Si (red), Fe (green), oxygen (yellow), and Ar (pink), overwritten on the corresponding HAADF-STEM image. The solid lines in each figure indicate the location of the bonding interface.

Fig. 2. (a) Low- and (b) high-magnified HAADF-STEM of nano-voids at a diamond/Si bonding interface annealed at 1000 °C. Spatial distribution of (c) Si, (d) carbon, (e) Fe, (f) oxygen, and (g) Ar atoms around the nano-void in (b).

Fig. 3. (a) Low- and (b) high-magnified HAADF-STEM of nano-voids at a Si/Si bonding interface annealed at 1000 °C. Spatial distribution of (c) Si, (d) Fe, and (e) Ar atoms around the nano-void in (b).



1
2
3
4
5
6
7 Fig.1.
8
9
10
11
12
13
14
15
16
17
18
19
20
21
22
23
24
25
26
27
28
29
30
31
32
33
34
35
36
37
38
39
40
41
42
43
44
45
46
47
48
49
50
51
52
53
54
55
56
57
58
59
60

Accepted Manuscript

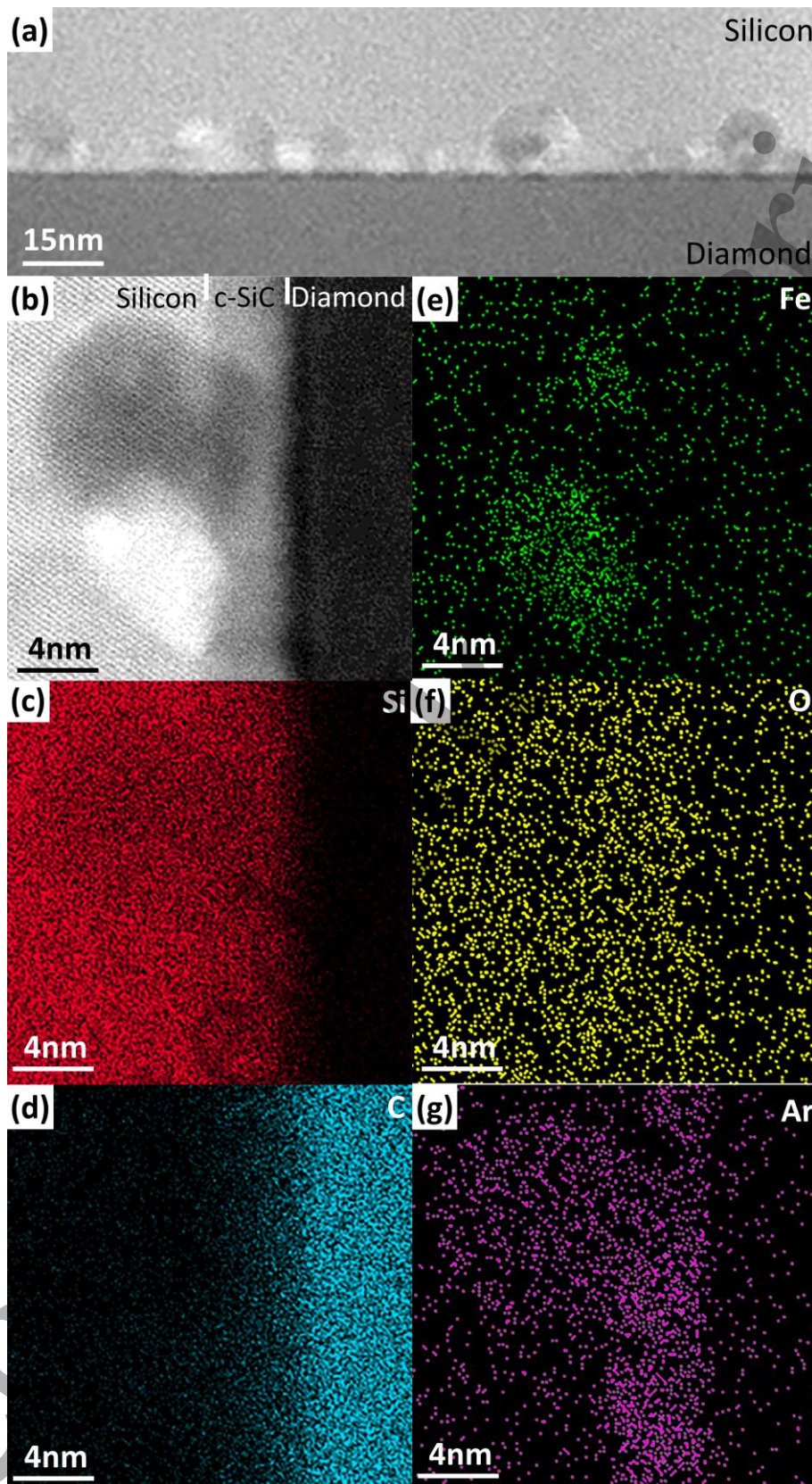


Fig.2

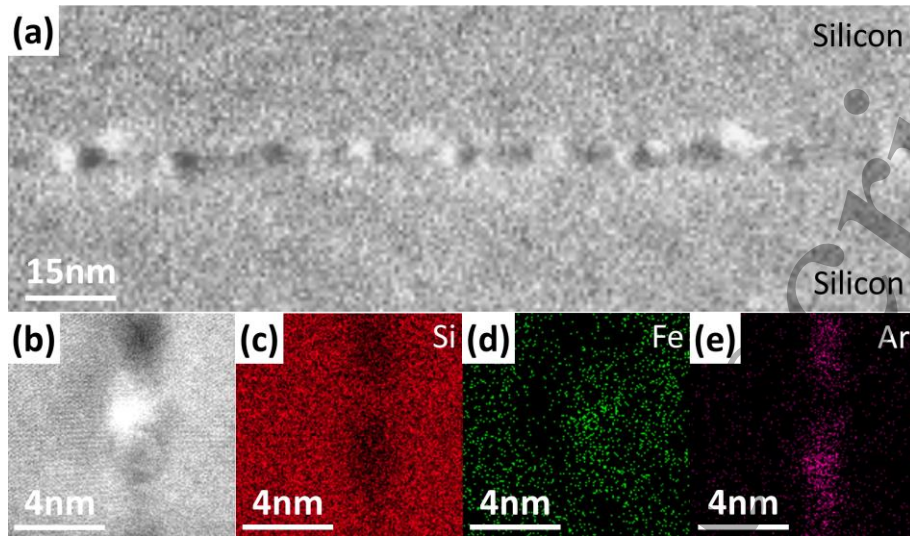


Fig.3